ACS APPLIED NANO MATERIALS

www.acsanm.org Article

A Holey 2D MoS_2-Based Membrane with Mo-Rich Edges for Water Desalination

Biswajit Mondal, Sudhin Rathnakumaran, Amrita Chakraborty, Pragin Chettiyankandy, Pillalamarri Srikrishnarka, Md Rabiul Islam, Jenifer Shantha Kumar, Ramesh Kumar, Sandeep Bose, Sooraj Kunnikuruvan,* and Thalappil Pradeep*

Cite This: https://doi.org/10.1021/acsanm.5c05244 Read Online

ACCESS | Metrics & More | Article Recommendations | Supporting Information

ABSTRACT: Developing thin-film composite membranes that simultaneously exhibit high water permeability and ion rejection (IR) remains a persistent challenge in desalination research. Here, we report the fabrication of polyamide (PA) membranes embedded with holey molybdenum disulfide nanosheets via controlled interfacial polymerization. The introduction of nanoscale Mo-rich pores within MoS_2 provides low-friction water transport channels, while maintaining effective ion exclusion. Systematic optimization of interfacial polymerization conditions—specifically monomer contact time of 60 s each and nanosheet loading of 0.01 wt % resulted in an optimal water flux (WF) of ∼96 L m^{-2} h^{-1} and IR of ∼99.4%, outperforming both pristine PA and nonporous MoS_2-based membranes. Molecular dynamics simulations revealed that water molecules align preferentially along hydrophilic Mo-edge sites, forming ordered, high-density transport channels responsible for the observed flux enhancement. Together, the experimental and computational results establish holey MoS_2-embedded PA membranes as a promising platform for next-generation nanofiltration and desalination technologies.

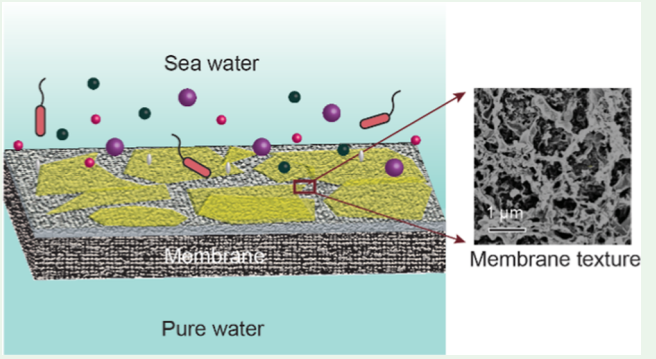

KEYWORDS: *Mo-rich holey MoS_2, ambient electrospray deposition, interfacial polymerization, membrane, desalination of water*

1. INTRODUCTION

Although water covers 75% of the surface of the Earth, producing fresh water is one of the most pressing global challenges of the 21st century. This crisis is exacerbated by rapid population growth, escalating industrial and agricultural demands, contamination of existing water resources, and the impacts of unprecedented climate change.[1−5] Since over 97.5% of Earth's water is contained in the oceans, desalination of seawater and brackish sources becomes indispensable to meet the growing demand for fresh water.[1] Among various desalination techniques, membrane-based separation techniques such as reverse osmosis (RO) has emerged as the most efficient and widely adopted method to produce clean water from seawater, brackish water, and various sources of wastewater. RO is favored due to its low energy consumption, modular operation, minimal use of chemical additives, and technological simplicity compared with conventional distillation-based approaches.[2,6] Although most of the available commercial membranes are composed of polysulfone (psf) and polyamide, alternative materials such as zeolite-based membranes and mesoporous ceramics have also been explored.[6,7] Despite their widespread applications, conventional polymeric nanofiltration membranes face several challenges including poor thermal stability, high sensitivity to acidic, basic, or organic solvent media, high energy requirement, lower WF, and low fouling resistance.[8,9] On the other hand, ceramic membranes, while offering excellent chemical and mechanical stability, are prohibitively expensive for large-scale implementation, and zeolite-based materials often suffer from inherently low permeation rates despite their structural advantages.[10,11]

To overcome these limitations, scientists have focused on exploring alternative materials and architectures. In recent years, two-dimensional (2D) materials have emerged as a compelling platform for the next-generation membranes for separation. Their atomically thin structure, precise nanocapillary channels between layers, and the possibility of engineered nanopores make them promising in the membrane technology due to high flux and high rejection.[12−14]

Received: November 16, 2025
Revised: November 23, 2025
Accepted: November 24, 2025

Scheme 1. Fabrication Process of the Membrane Used in This Study

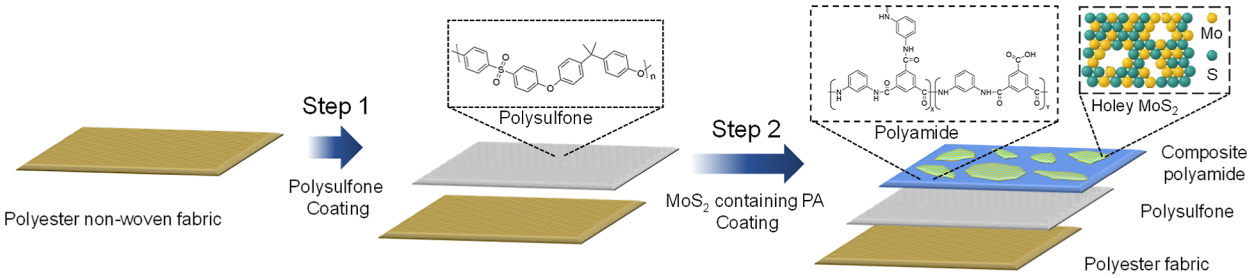

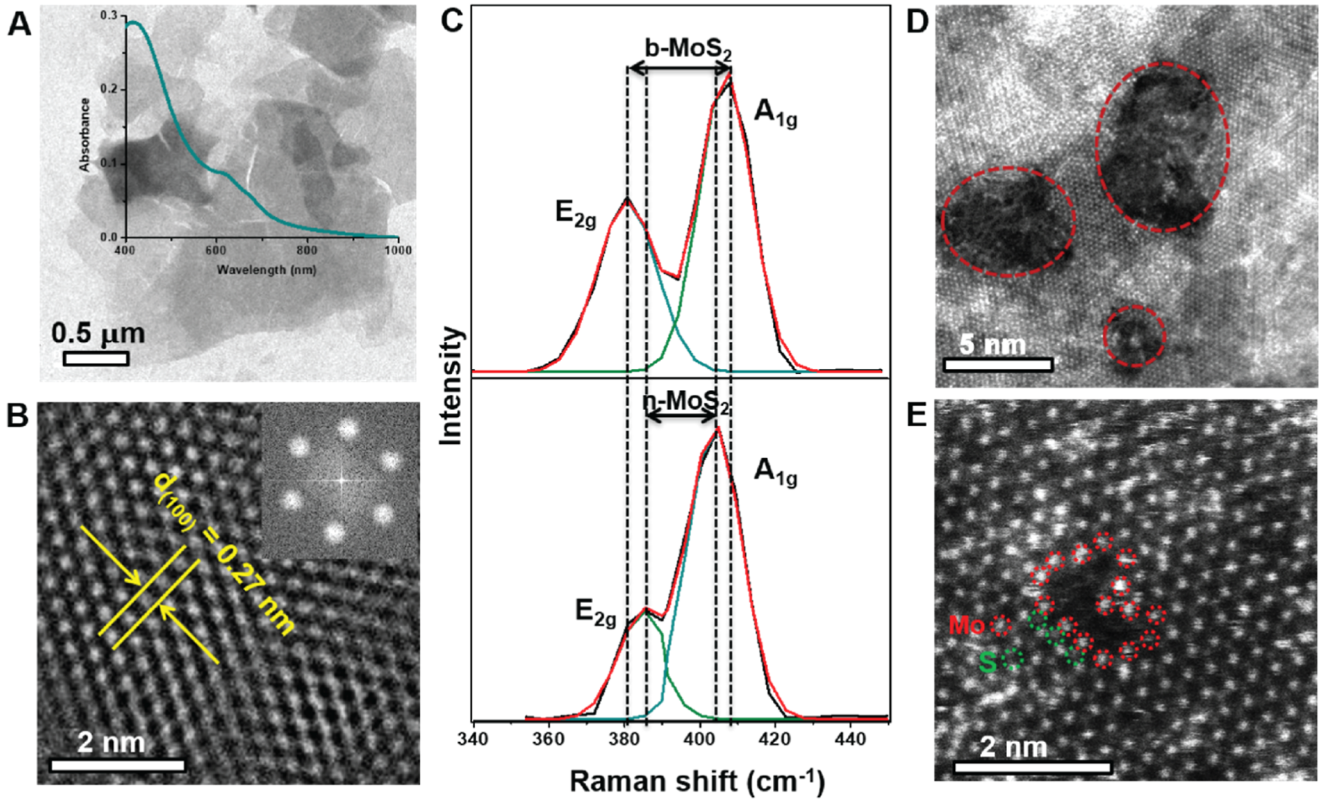

Figure 1. (A) TEM image of the as-synthesized MoS_2 NSs. The inset shows the corresponding UV/vis absorption spectrum. (B) HRTEM image of a MoS_2 NS and the corresponding fast Fourier transform pattern shown in the inset of (B). (C) Raman spectra collected from the MoS_2 NSs (n-MoS_2) and bulk MoS_2 (b-MoS_2). (D) Scanning transmission electron microscopy (STEM) image of a holey MoS_2 NS collected after electrospray of Ag^+ ions, and (E) HAADF STEM of the same showing a Mo-enriched edge. Red circles in image (E) denote Mo, and the green circles represent S.

Continuous water channels form either through intrinsic interlayer spacings or deliberately perforated nanopores, enabling control over molecular and ionic transport via steric, electrostatic, and interfacial interactions. Among 2D materials, MoS_2 nanosheets (NSs) are found superior over other 2D materials in the membrane technology due to their excellent mechanical properties, tunable surface chemistry, high fouling resistance, and stability in the aqueous environments.[15−18] Unlike oxidized graphene derivatives, the absence of oxygenated functional groups in MoS_2 provides reduced resistance for the transport of water molecules and resists swelling in aqueous media[15,19] Existing reports demonstrate that the MoS_2-based membrane has a promising separation efficiency and excellent WF, precisely 2−5 times higher than the GO-based membranes under similar experimental conditions.[20] MoS_2-based RO membranes show enhanced IR performance due to the presence of negative charge on MoS_2 NSs, which repel the ions of salt. Furthermore, exfoliated MoS_2 NSs give rise to increased hydrophilicity on the membrane's surface. High negative charge and hydrophilic sites provided by Mo/S atoms of MoS_2 NSs can effectively change the physicochemical properties of the membrane such as roughness, electrostatic charge, and hydrophilicity, which influence IR, water permeation rate, and membrane fouling.[21] The layered structure of MoS_2 permits the formation of nanocapillary channels when stacked and the potential to introduce nanopores offers a route to improve both flux and rejection.[22,23]

Molecular dynamics (MD) studies have been used to study ion/water permeation through nanoporous MoS_2 membranes. In a seminal study, Heiranian et al. demonstrated that single-layer MoS_2 NSs containing nanopores show enhanced water permeation rate compared to graphene nanopores under the same conditions.[24] The nanopores decorated with Mo atoms

https://doi.org/10.1021/acsanm.5c05244
ACS Appl. Nano Mater. XXXX, XXX, XXX−XXX

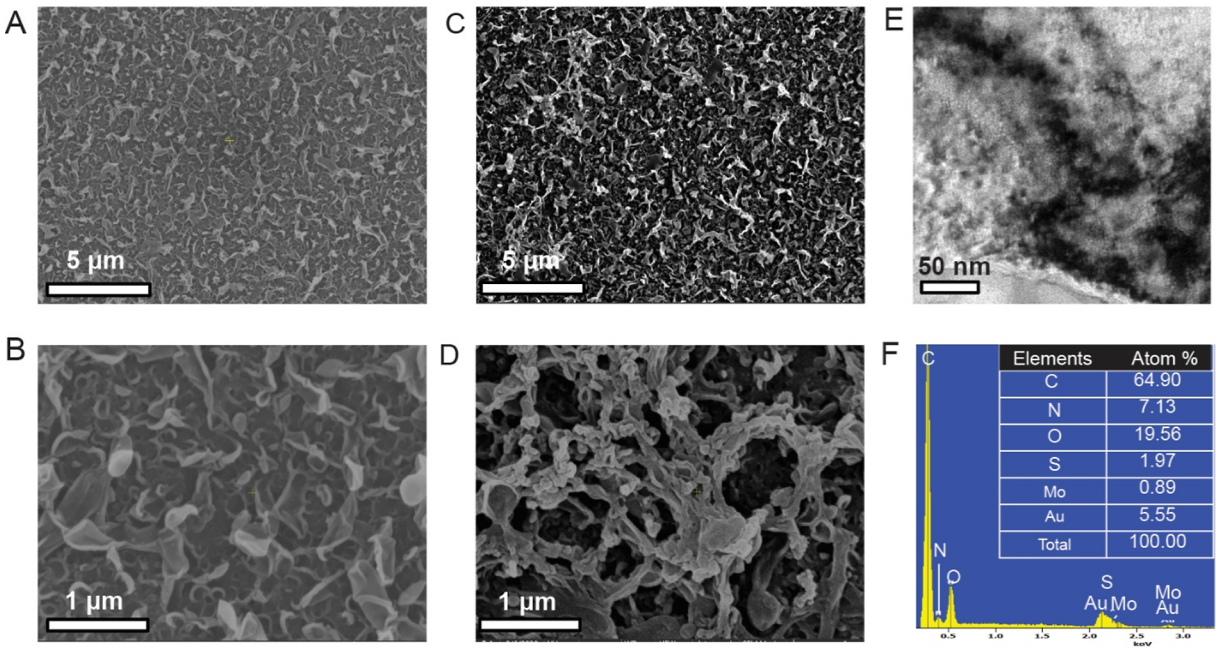

Figure 2. FESEM images of blank membrane (A,B) and the membrane containing 0.01 wt % holey MoS_2 (C,D) at different magnifications after gold sputtering. (E) TEM image of the holey MoS_2-based membrane. EDS elemental analysis of the corresponding membrane is shown in (F).

show the highest flux due to the higher density and velocity of water inside the Mo-pores.[24] MD and first-principles simulations have since revealed how variations in edge chemistry, pore size, ion−pore interactions, hydration, and applied pressure affect desalination efficiency.[25−29] Recent MD studies have shown that Mo-rich edges promote water restructuring and reduce energy barriers which facilitate water transport.[24] Meanwhile, comparative theoretical study has revealed that MoS_2 nanopores outperform graphene-based analogues under some conditions.[24,30]

Despite significant progress, the experimental realization of scalable, defect-controlled, nanopore-engineered MoS_2 remains highly challenging. Existing demonstrations are often confined to small membrane areas or depend on costly, high-precision fabrication methods—such as electron-beam sculpting, ion-beam drilling, or focused ion beam processing—that lack scalability.[31−33] Although vacuum filtration and chemical vapor deposition approaches have been used to produce MoS_2 thin films and laminar membranes,[20,34] control over pore chemistry and antifouling behavior remains limited. Consequently, there is a pressing need for a scalable and cost-effective MoS_2-based RO membrane that combines engineered nanopores with high flux, selectivity, and fouling resistance.

In this work, we combine our experimental membrane fabrication with corroborative MD simulations to dissect the roles of pore chemistry and nanosheets architecture in water/ion transport. We demonstrated a facial, ambient, solution-based home-grown method for Mo-rich, holey MoS_2 nanosheets and their integration into the polyamide membranes. Specifically, a copolymerization method was used to fabricate the membrane, where holey MoS_2 NSs were added during the polymerization process to increase the performance of the membrane (schematic 1). We systematically tuned the nanosheet loading, monomer contact time, and pore chemistry and correlated these parameters with desalination performance and fouling resistance. Benchmarking against control membranes, we demonstrate that holey-MoS_2-based membranes exhibit superior performance. This work advances the practical realization of high-performance 2D-material membranes by coupling scalable synthesis with mechanistic insights into pore effects and surface interaction.

2. RESULTS AND DISCUSSION

2.1. Characterization of MoS_2 and Holey MoS_2 NSs. MoS_2 NSs were first synthesized using a standard chemical exfoliation method.[35,36] Figure 1 summarizes the essential characterization data of as-synthesized NSs. Transmission electron microscopy (TEM) and HRTEM images of the as-synthesized NSs are shown in Figure 1A,B, respectively. Their structural integrity was further assessed using Raman spectroscopy. The characteristic E_2g and A_1g vibrational modes of 2D MoS_2 were clearly observed, and the reduced peak separation between these modes for MoS_2 NSs (n-MoS_2) indicates the successful exfoliation of bulk MoS_2 (b-MoS_2) to its nanoscale form (Figure 1C).[37,38] Mo-rich holey MoS_2 NSs were subsequently prepared using a facile, cost-effective, ambient, solution-based method developed in our group.[39] In this process, Ag^+ ions were electrosprayed on an aqueous suspension of chemically synthesized MoS_2 NSs. During deposition, Ag^+ ions react with the NSs to form Ag_2S, leaving behind Mo-enriched nanopores within the sheets (Figure 1D,E).[39,40] In Figure 1E, Mo and S atoms are highlighted with red and green dotted circles, respectively. UV/vis absorption spectrum and Raman spectroscopic data show no significant deviation from those of pristine MoS_2 NSs, confirming that the introduction of nanopores does not alter the intrinsic electronic structure of the material.

2.2. Characterization of Membranes. After the fabrication of membranes (discussed in the Experimental Section), they were characterized using various microscopic and spectroscopic techniques. Surface morphology and roughness of the membranes were observed with field emission scanning electron microscopy (FESEM) (Figure 2A−D) after gold sputtering. The incorporation of holey MoS_2 nanosheets

https://doi.org/10.1021/acsanm.5c05244
ACS Appl. Nano Mater. XXXX, XXX, XXX−XXX

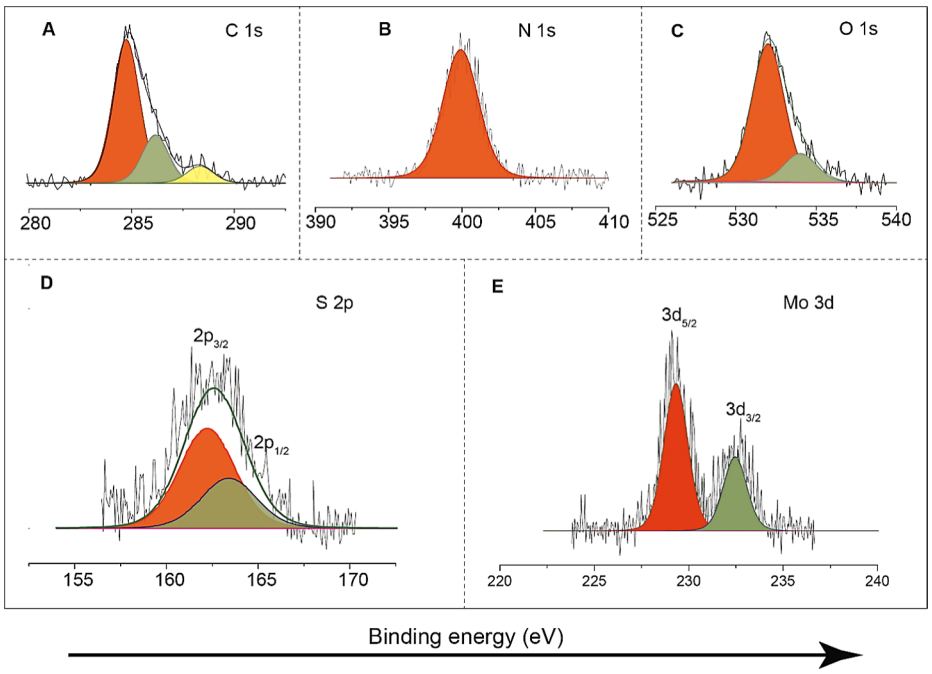

Figure 3. XPS of the membrane containing 0.01 wt % of holey MoS_2. (A–E) XPS in the C 1s, N 1s, O 1s, S 2p, and Mo 3d regions, respectively.

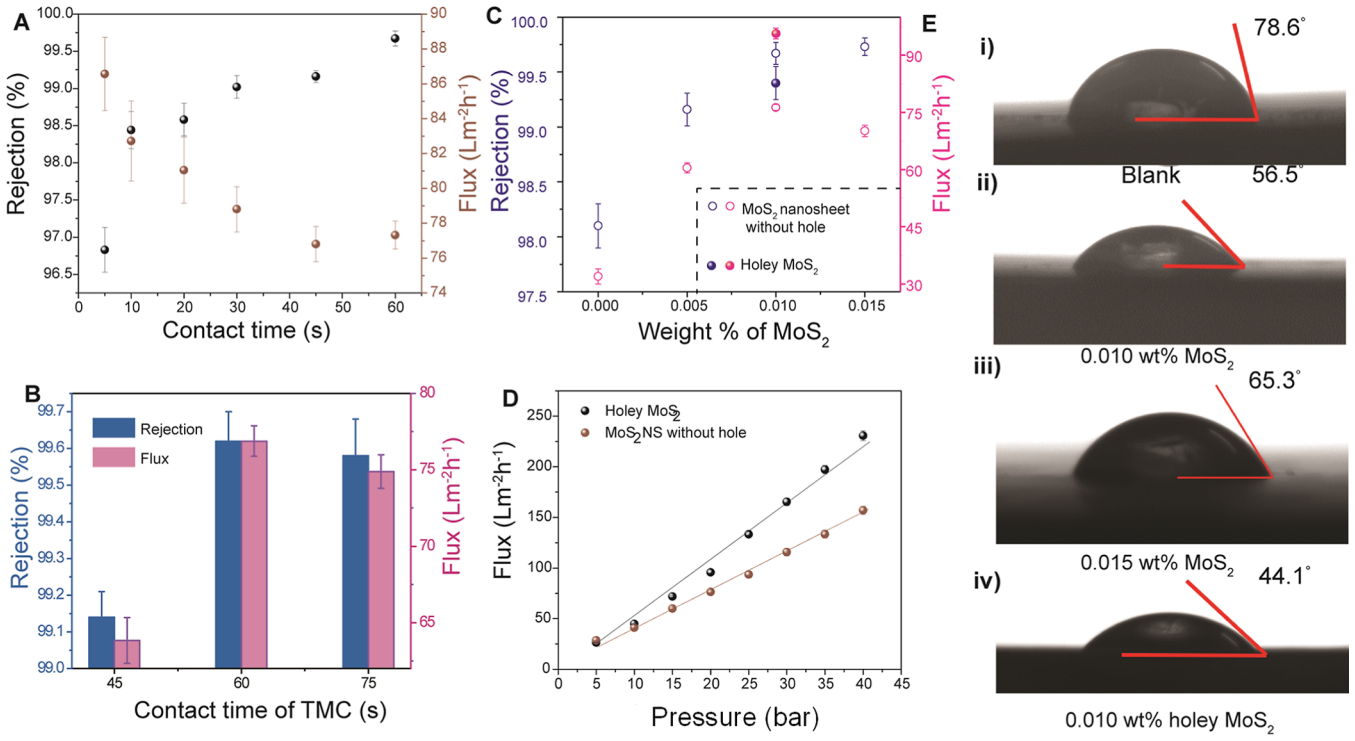

Figure 4. (A) Change in flux and rejection (%) with the change in contact time, and (B) effect of permeation rate and rejection performance with variation of contact time of TMC solution. (C) MoS_2 concentration-dependent rejection performance and water permeation rate, and (D) variation of flux as a function of pressure. (E) Water contact angle on blank membrane (i), membranes containing different amounts of MoS_2 (ii,iii), and holey MoS_2-based membrane (iv). (A–C) contain two *Y* axes (rejection and flux).

(NSs) induced a noticeable change in surface texture—from a distinctly leaf-like morphology in the blank polyamide membrane (without MoS_2 NSs, abbreviated hereafter as bM, Figure 2A,B) to less leaf-like and more nodular structure for the membrane containing 0.01 wt % of holey MoS_2 NSs, abbreviated hereafter as 0.01 wt % $hMoS_2M$ (Figure 2C,D). Among the prepared membranes, the 0.01 wt % $hMoS_2M$ exhibited the best performance and was therefore selected for detailed TEM analysis (Figure 2E). The surface morphology of holey MoS_2-based membranes (abbreviated hereafter as $hMoS_2M$) and those incorporating nonporous MoS_2 NSs (abbreviated hereafter as MoS_2M) were found to be comparable when equivalent nanosheet loadings were used (Figure S1). The presence of MoS_2 NS on the membrane

https://doi.org/10.1021/acsanm.5c05244
ACS Appl. Nano Mater. XXXX, XXX, XXX−XXX

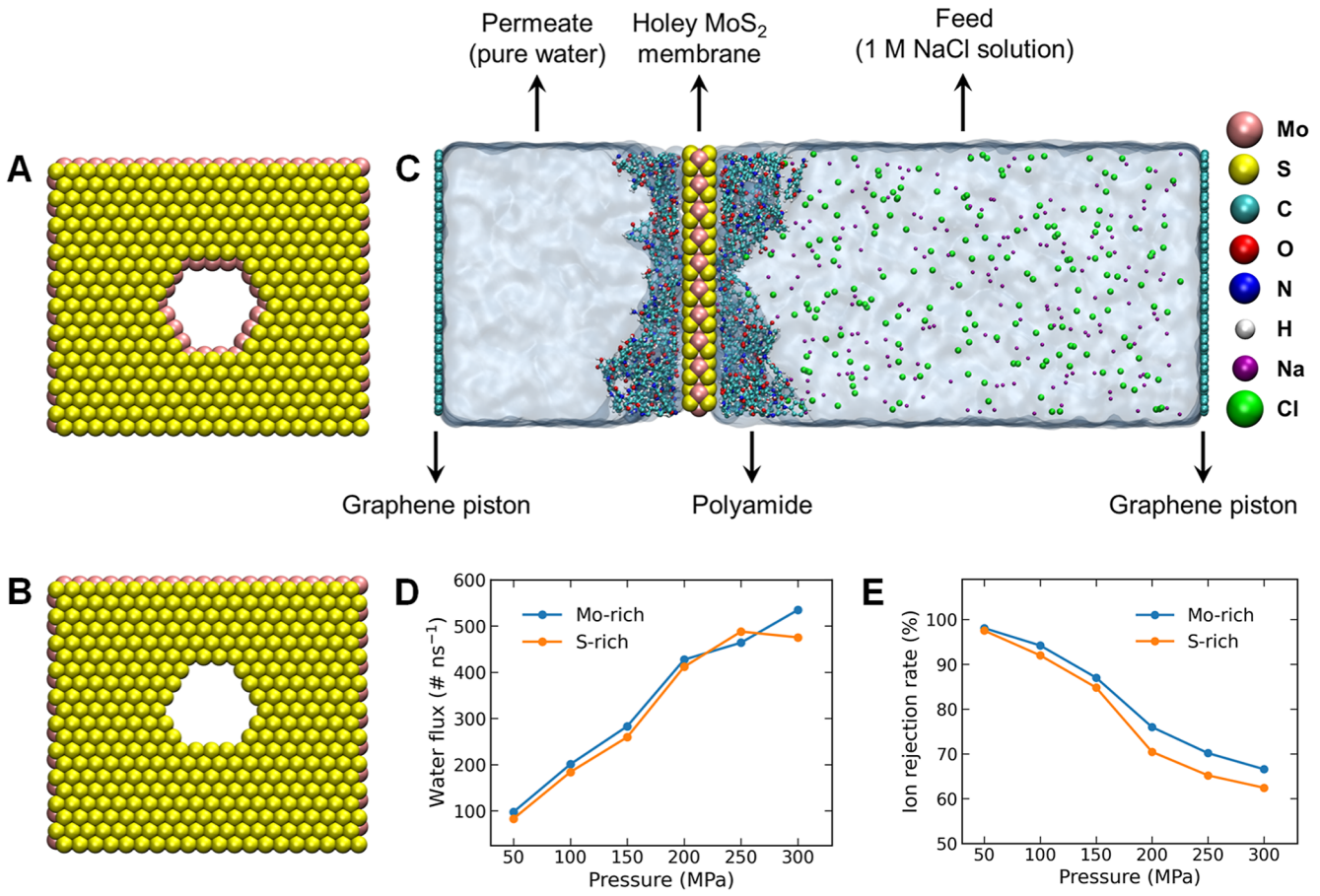

Figure 5. $hMoS_2$NSs with (A) Mo-rich and (B) S-rich pores used in MD simulations. (C) Side view of the representative MD setup showing feed (1 M NaCl), permeate (pure water), $hMoS_2$NS, PA, and graphene pistons. (D) WF and (E) IR rates at different applied pressures for the Mo-rich and S-rich $hMoS_2$Ms.

surface was confirmed by energy-dispersive spectroscopy (EDS) analysis in TEM (Figure 2F). At higher loadings, MoS_2 NSs tended to aggregate owing to their high surface energy in the nonpolar organic solvent (Figure S2).

X-ray photoelectron spectroscopy (XPS) was performed to further analyze the surface composition and chemical states. Spectra in the C 1s, O 1s, N 1s, S 2p, and Mo 3d regions are presented in Figure 3. The Mo 3d region shows two peaks at 229.3 and 232.4 eV corresponding to $3d_{5/2}$ and $3d_{3/2}$, respectively (Figure 3E). The two peaks at 161.6 and 162.9 eV correspond to $2p_{3/2}$ and $2p_{1/2}$ of S^{2-} of MoS_2 (Figure 3D), which confirms that there is no chemical change in holey MoS_2 NS after the fabrication of the membrane. The sensitivity of XPS even at such a low loading suggests the existence of $hMoS_2$ on the surface of the membrane.

The FT-IR spectrum of $hMoS_2$M (Figure S3) displays all the characteristic peaks of polyamide. The broad band between 3200 and 3500 cm^{-1} arises from N−H and O−H stretching vibrations. Peaks at 1660, 1580, and 1150 cm^{-1} are attributed to C═O stretching, aromatic C═C stretching, and C−N stretching, respectively. The bands at 1543 and 832 cm^{-1} correspond to N−H bending and aromatic C−H bending modes. Additionally, a weak peak around 460 cm^{-1} is assigned to Mo−S stretching, further confirming the incorporation of MoS_2 NSs within the membrane structure.

2.3. Performance of Membranes. The desalination performance of the fabricated membranes was systematically evaluated using a laboratory-scale RO setup (Figure S4). The influence of interfacial polymerization parameters—specifically, the contact time between the aqueous *m*-phenylenediamine (MPD) solution and the 1,3,5-benzenetricarbonyl trichloride (TMC) solution in hexane—and MoS_2 NS loadings were quantitatively analyzed in terms of WF and IR.

The contact time between the two monomer phases determines the thickness and cross-linking density of the polyamide (PA) layer, which in turn control both flux and rejection. The variation in WF and IR performance was measured as a function of contact time of both MPD solution and TMC solution (Figure 4A). An optimal balance between WF and IR was achieved when the contact time for each monomer was set to 60 s. Shorter exposure times resulted in a thinner, loosely cross-linked PA layer that permitted partial ion leakage, thereby lowering IR. In another set of experiments, the contact time of TMC solution was varied (45, 60, and 75 s); while maintaining MPD exposure at 60 s, a similar trend was observed (Figure 4B). Increasing TMC exposure to 60 s yielded the maximum WF and IR, whereas prolonged contact (75 s) reduced flux, likely due to excessive cross-linking and reduced pore connectivity. These observations confirm that the interfacial polymerization conditions govern the morphology and permeability of the selective layer.

The effect of MoS_2 NS loadings on the membrane performance was next investigated by varying the nanosheet concentration from 0 to 0.015 wt % in the polymerization mixture (Figure 4C). Compared to the blank membrane, MoS_2 NS loadings significantly enhanced water permeability, reach-

https://doi.org/10.1021/acsanm.5c05244
ACS Appl. Nano Mater. XXXX, XXX, XXX−XXX

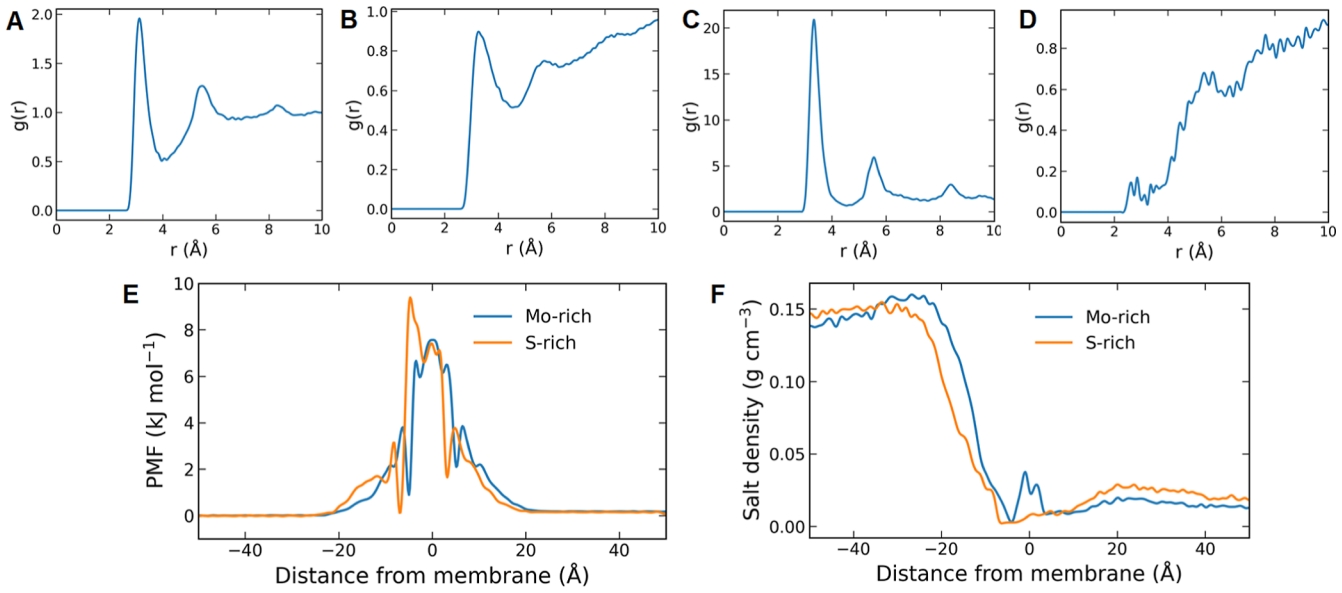

Figure 6. RDF plots between (A) pore Mo atoms of Mo-rich $hMoS_2M$ and O atoms of water, (B) pore S atoms of S-rich $hMoS_2M$ and O atoms of water, (C) pore Mo atoms of Mo-rich $hMoS_2M$ and salt ions, and (D) pore S atoms of S-rich $hMoS_2M$ and salt ions, computed from RO simulations at 200 MPa. (E) 1-D PMF profiles of water molecules, and (F) salt ion density profiles along the *Z*-direction, computed from RO simulations at 200 MPa.

ing a maximum at 0.01 wt % MoS_2. This improvement is attributed to the formation of additional nanocapillary channels and increased hydrophilicity imparted by the exposed Mo−S surface sites. However, further loading led to a decline in flux—possibly due to nanosheet agglomeration within the PA matrix that increased transport resistance. Simultaneously, the IR improved with increasing MoS_2 content, driven by stronger electrostatic repulsion between negatively charged MoS_2 surfaces and anionic species in saline feed, as well as by a denser polymer network induced by nanosheet−polymer interactions. Overall, 0.01 wt % MoS_2M exhibited the best trade-off between flux and rejection. Further enhancement was achieved by introducing Mo-rich nanopores (2−8 nm) within the nanosheets. The holey MoS_2 membrane ($hMoS_2M$) at 0.01 wt % loading achieved a WF of ∼96 L m^{-2} h^{-1}—*a* ∼ 26% increase compared to the nonholey MoS_2 membrane under identical testing conditions. Simultaneously, salt rejection of ∼99.4% indicates that nanopore introduction does not compromise selectivity. This improvement can be rationalized by the unique water structuring as supported by MD simulations. The hydrophilic Mo sites at the pore edges attract and orient water molecules, creating low-friction transport channels that facilitate rapid and efficient water flow without compromising ion selectivity.

Water fluxes through the membranes as a function of externally applied pressure are presented in Figure 4D. To assess the relative performance, $hMoS_2M$ was compared with the MoS_2M, which had already demonstrated promising water permeation characteristics. Across the entire pressure range tested, $hMoS_2M$ consistently exhibited higher WF than MoS_2M. The WF increased linearly with applied pressure, indicating stable membrane integrity and consistent transport behavior, while the IR remained nearly constant throughout the tested pressure range (Figure S5).

The higher water permeation rate observed for 0.01 wt % $hMoS_2M$ compared to the other membranes (MoS_2M and bM) can be explained in terms of its altered surface morphology and roughness, which together change surface hydrophilicity. Figure 4E shows the variation in water contact angles on different membranes. A significant decrease in contact angle for 0.01 wt % $hMoS_2M$ compared to the bM indicates enhanced surface wettability upon incorporation of nanoporous MoS_2 NSs. To further examine how MoS_2 nanosheets influence the physicochemical properties of the membrane, a series of membranes was fabricated with varying MoS_2 loadings, and their water contact angles were measured (Figure 4E(i−iii)). As the MoS_2 concentration increased up to 0.01 wt %, the contact angle progressively decreased due to the greater exposure of polar Mo−S sites at the surface. However, at higher loadings, the contact angle increased again, likely due to nanosheet aggregation and the intrinsically lower hydrophilicity of MoS_2 compared with the polyamide matrix.

2.4. MD Simulations. To scrutinize the effect of Mo-rich and S-rich pores on the RO performance of the $hMoS_2Ms$, classical MD simulations were performed. Hexagonal nanopores were introduced into MoS_2 NSs to create the holey MoS_2 NSs ($hMoS_2NSs$) with either Mo-rich or S-rich pore edges (Figure 5A,B). The lateral dimensions of the NSs were 6.21 nm × 5.47 nm, and nanopores with a diameter of about 2 nm were used in the RO simulations. The RO setup (Figure 5C) includes a 1 M NaCl solution in the feed layer and pure water in the permeate layer. In the initial structure, the feed layer (11.2 nm) consists of 10,075 water molecules, 181 Na^+ ions, and 181 Cl^- ions, while the permeate layer (5.6 nm) consists of 4671 water molecules. MD simulations were performed using the LAMMPS software package,[41] and visualization and analyses were carried out using the Visual Molecular Dynamics (VMD) program.[42] Information on the force field parameters and additional simulation details can be found in the "Computational details" section of the Supporting Information.

The performances of Mo-rich and S-rich $hMoS_2Ms$ were compared in terms of the computed WF and IR. Furthermore, the local environment and interfacial interactions were

https://doi.org/10.1021/acsanm.5c05244
ACS Appl. Nano Mater. XXXX, XXX, XXX−XXX

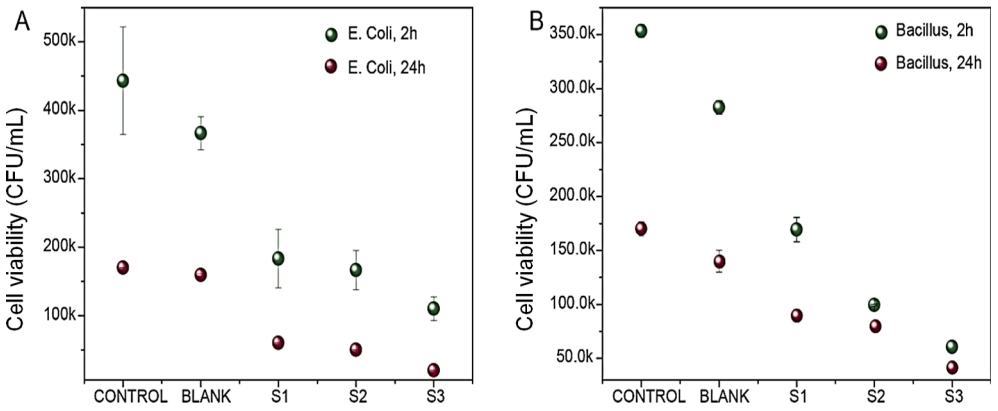

Figure 7. Antifouling experiment with *E. coli* (A) and *B. subtilis* (B) where incubation times are 2 and 24 h. Labels S1, S2, and S3 refer to the loading of MoS_2 (see the text).

analyzed to gain insights into the structural and chemical features contributing to their RO effectiveness. The RO simulations indicate that the equilibrated membrane structures (Figure S9) had a nonuniform thickness varying from 20 to 40 Å. The PA oligomers showed strong affinity toward the $hMoS_2$NSs but were not found inside the nanopore region. The S atoms of the $hMoS_2$NSs and the H atoms of the PA oligomers had the closest interaction distance of about 2.5 Å. During the RO simulations, the number of filtered water molecules increased linearly with time (Figure S10), indicating that the system has attained the stationary state. The WF and IR rates were calculated using the equations below

$$\mathrm{WF} = \frac{N_{\mathrm{water}}}{t}$$

where N_{water} is the number of permeated water molecules and t is the simulation time in ns.

$$\mathrm{IR}\ (\%) = \frac{N_{\mathrm{ion}} - N_{\mathrm{ion}}^{\mathrm{P}}}{N_{\mathrm{ion}}} \times 100$$

where N_{ion} is the total number of ions in the feed, and $N_{\mathrm{ion}}^{\mathrm{P}}$ is the number of ions that permeated through the membrane. The WF (Figure 5D) was comparable for the membranes, with the Mo-rich $hMoS_2M$ exhibiting slightly higher flux at most of the applied pressures and a significantly higher flux at 300 MPa. The IR (Figure 5E) was consistently superior for the Mo-rich $hMoS_2M$ across all applied pressures, and the difference became more pronounced at higher pressures.

The radial distribution function (RDF) plots[43] were computed between the O atoms of water molecules and atoms along the internal pore edges (Mo atoms for Mo-rich $hMoS_2M$ and S atoms for S-rich $hMoS_2M$). The first coordination shells of the pore Mo and pore S atoms were found to be centered around 3.1 Å and 3.2 Å, respectively (Figure 6A,B). A higher $g(r)$ for Mo−O corresponding to the first coordination shell indicates a higher probability of finding the water molecules near the pore edges in the case of Mo-rich $hMoS_2M$ (Figure S11). This localized water density at the pore region of the Mo-rich $hMoS_2M$ could be responsible for its slightly enhanced water permeability, which is consistent with the computed water fluxes (Figure 5D).

The RDF plots between the pore atoms and salt ions show a prominent peak in the Mo-salt ion RDF (Figure 6C) for the Mo-rich $hMoS_2M$ at r = 3.3 Å, whereas the corresponding $g(r)$ for S-salt ion (Figure 6D) for the S-rich $hMoS_2M$ was found to be weak. This peak in the Mo-salt RDF can be attributed to the strong interactions between the Mo atoms and Cl^- ions (Figure S12A). The comparatively lower $g(r)$ for the first coordination shell of S-salt ion interactions is in line with the weak S−Cl^- interactions (Figure S12B). The sustained Mo−Cl^- interactions (Figure S13) and the repulsive Mo−Na^+ ions interactions could be responsible for the enhanced IR observed for Mo-rich $hMoS_2M$. The RDF plots between water O atoms and the O atoms of the PA (Figure S14A) showed no significant differences, though slightly higher $g(r)$ values were observed for the S-rich $hMoS_2M$. In contrast, RDF plots between water O atoms and the N atoms of the PA (Figure S14B) showed slightly stronger interactions in the Mo-rich $hMoS_2M$ as compared to S-rich $hMoS_2M$. A similar trend was observed for salt ions, i.e., the O atoms in S-rich $hMoS_2M$ had slightly stronger interactions with the ions compared to the O atoms in Mo-rich $hMoS_2M$ (Figure S14C), while the N atoms in Mo-rich $hMoS_2M$ exhibited slightly stronger interactions with salt ions compared to those of S-rich $hMoS_2M$ (Figure S14D).

To complement the structural insights from RDF analysis and to assess the barriers for water transport, potential of mean force (PMF) profiles were computed to compare the permeability of $hMoS_2$Ms. The one-dimensional PMF for water molecules along the Z-direction (Figure 6E) from the center of the membrane was computed, perpendicular to the NS surface, using the relation below

$$\mathrm{F}(r) = -RT\ln \rho(r)$$

where R is the gas constant, T is the temperature, and $\rho(r)$ is the density of water at a distance r from the membrane.[44]

The 1-D PMF computed from RO simulations at 200 MPa indicates a comparable free-energy barrier for S-rich $hMoS_2M$ (9 kJ mol^{-1}) and Mo-rich $hMoS_2M$ (8 kJ mol^{-1}). This is in line with the comparable WF observed for Mo-rich and S-rich $hMoS_2$Ms (Figure 5D) at 200 MPa. Furthermore, the analysis of salt ion density profiles along the Z-direction (Figure 6F) indicates a noticeably lower ion density in the permeate region for the Mo-rich $hMoS_2M$ as compared to the S-rich $hMoS_2M$. This is in line with its higher IR rates observed in the RO simulations (Figure 5E). Distinct salt ion density peaks were observed at the pore region of the Mo-rich $hMoS_2$NS. This can be ascribed to stronger interactions between the ions and the Mo atoms at the edges of the pore, thereby reducing ion permeation.

https://doi.org/10.1021/acsanm.5c05244
ACS Appl. Nano Mater. XXXX, XXX, XXX−XXX

To investigate the effect of the MoS_2 NSs on the filtration properties of $hMoS_2Ms$, an independent simulation involving bM, composed solely of PA oligomers (Figure S15), was performed. To model bM, 12 PA oligomers were used, ensuring a thickness comparable to the $hMoS_2Ms$. Here, four C atoms from each oligomer were fixed during the RO simulations to keep the center of mass of bM fixed in the *Z*-direction, and the simulations were performed at 100 MPa. The RO simulation showed an IR of 89.2% and a WF of 353 # ns^{-1} for bM, compared to 94.2% and 201 # ns^{-1} for the Mo-rich $hMoS_2M$. This shows that the MoS_2 NS plays a significant role in enhancing salt IR as the rejection rate is considerably lower in the absence of the NS. The higher WF in the bM can be attributed to the modeled concentration (200.32 wt %) of MoS_2 NSs in the $hMoS_2M$, which is much higher than the optimal value of 0.01 wt % used in our experiments.

2.5. Antifouling Properties of Membranes. Fouling of membranes by microorganisms is the major limiting factor in the membrane technology, resulting in a decrease in membrane selectivity and water permeation rate, an increase in energy consumption, and a decrease in membrane lifetime. Although pretreatment of feedwater can reduce the number of microorganisms but cannot remove the bacterial cells completely, which colonize and form biofilms on the membrane surface resulting in blockage of nanocapillaries present in the membrane. Therefore, it is very important to address this problem. Foulants are less likely to adhere to the MoS_2 NS surfaces due to the extremely low friction.[45] Besides, in our previous report, we demonstrated that holey MoS_2 NS exhibits excellent antibacterial property.[39] Therefore, antifouling properties of both MoS_2M and $hMoS_2M$ were tested with both Gram-positive (*Bacillus subtillis*) (Figure 7A) and Gram-negative (Escherichia coli) (Figure 7B) bacteria. The bacterial cells were incubated (2 and 24 h) with 1 cm × 1 cm pieces of the membranes, and the number of live cells after incubation was counted by plating the cells on nutrient agar plates. In comparison to a bM, $hMoS_2M$ shows the highest reduction in the bacteria count, and the antifouling efficiency increases with the amount of loading of MoS_2 (S1 = 0.01 wt % of MoS_2; S2 = 0.015 wt % of MoS_2; and S3 = 0.01 wt % of holey MoS_2).

3. CONCLUSION

In summary, we have successfully designed and fabricated holey MoS_2-incorporated thin-film composite membranes that demonstrate a synergistic improvement in water permeability and IR. The performance enhancement arises from three cooperative effects: (i) optimized interfacial polymerization conditions (60 s/60 s) that ensure uniform, defect-free PA layer formation; (ii) MoS_2 nanosheet incorporation (0.01 wt %) that increases surface hydrophilicity and introduces additional nanocapillary pathways; and (iii) nanoscale pores within MoS_2 that promote fast, directional water transport while preserving charge-based ion exclusion. The best-performing membrane achieved a WF of ∼96 L m^{-2} h^{-1} and NaCl rejection of ∼99.4%, confirming the potential of holey MoS_2 as a structural and functional modifier for high-performance RO membranes. MD simulations further support the experimental observations by elucidating how Mo-rich pore edges facilitate low-friction water flow through selective membrane−water interactions. Stabilizing Mo−Cl^- interactions and repulsive Mo−Na^+ interactions could be responsible for the superior IR in the case of Mo-rich $hMoS_2M$. The lower IR exhibited by bM in MD simulation highlights the critical role of MoS_2 NSs in enhancing membrane performance for effective RO filtration. Antifouling properties of the membrane were also tested with both Gram-positive and Gram-negative bacteria, and it was observed that holey MoS_2-based membranes show excellent antifouling properties due to their very low friction and fascinating disinfection property. This study not only provides a scalable route for engineering defect-tolerant, high-flux membranes but also delivers a mechanistic understanding of transport in 2D-material-assisted PA layers. The combined experimental−computational framework presented here offers valuable design principles for developing next-generation nanocomposite membranes tailored for sustainable desalination and water purification.

■ ASSOCIATED CONTENT

Supporting Information

The Supporting Information is available free of charge at https://pubs.acs.org/doi/10.1021/acsanm.5c05244.

Details of chemicals used; synthesis of MoS_2 NS; preparation of Mo-rich holey MoS_2 NS; fabrication of membranes; FESEM images of $hMoS_2M$, MoS_2M, and 0.015 wt % $hMoS_2M$; photograph of the setup used; pressure-dependent IR performance; computational details; structure of PA monomers and oligomers; simulation boxes; various RDF plots; MD snapshots of pore regions; and equilibrated membrane structures (PDF)

■ AUTHOR INFORMATION

Corresponding Authors

Sooraj Kunnikuruvan − *Department of Chemistry and Centre for Atomistic Modelling and Materials Design & Centre for Molecular Materials and Functions, Indian Institute of Technology Madras, Chennai 600036, India;* orcid.org/0000-0002-6734-4786; Email: soorajk@iitm.ac.in

Thalappil Pradeep − *DST Unit of Nanoscience (DST UNS) and Thematic Unit of Excellence (TUE), Department of Chemistry, Indian Institute of Technology Madras, Chennai 600036, India;* orcid.org/0000-0003-3174-534X; Email: pradeep@iitm.ac.in

Authors

Biswajit Mondal − *DST Unit of Nanoscience (DST UNS) and Thematic Unit of Excellence (TUE), Department of Chemistry, Indian Institute of Technology Madras, Chennai 600036, India*

Sudhin Rathnakumaran − *Department of Chemistry, Indian Institute of Technology Madras, Chennai 600036, India*

Amrita Chakraborty − *DST Unit of Nanoscience (DST UNS) and Thematic Unit of Excellence (TUE), Department of Chemistry, Indian Institute of Technology Madras, Chennai 600036, India; Department of Chemistry, BITS Pilani Hyderabad Campus, Telangana 500078, India*

Pragin Chettiyankandy − *Department of Chemistry, Indian Institute of Technology Madras, Chennai 600036, India*

Pillalamarri Srikrishnarka − *DST Unit of Nanoscience (DST UNS) and Thematic Unit of Excellence (TUE), Department of Chemistry, Indian Institute of Technology Madras, Chennai 600036, India;* orcid.org/0000-0001-5187-6879

Md Rabiul Islam − *DST Unit of Nanoscience (DST UNS) and Thematic Unit of Excellence (TUE), Department of*

https://doi.org/10.1021/acsanm.5c05244
ACS Appl. Nano Mater. XXXX, XXX, XXX−XXX

Chemistry, Indian Institute of Technology Madras, Chennai 600036, India; orcid.org/0000-0001-6454-4013

Jenifer Shantha Kumar − *DST Unit of Nanoscience (DST UNS) and Thematic Unit of Excellence (TUE), Department of Chemistry, Indian Institute of Technology Madras, Chennai 600036, India;* orcid.org/0009-0003-7502-7005

Ramesh Kumar − *DST Unit of Nanoscience (DST UNS) and Thematic Unit of Excellence (TUE), Department of Chemistry, Indian Institute of Technology Madras, Chennai 600036, India*

Sandeep Bose − *DST Unit of Nanoscience (DST UNS) and Thematic Unit of Excellence (TUE), Department of Chemistry, Indian Institute of Technology Madras, Chennai 600036, India;* orcid.org/0000-0002-3471-5392

Complete contact information is available at: https://pubs.acs.org/10.1021/acsanm.5c05244

Author Contributions

B.M. planned and designed the whole project. He synthesized MoS_2 NS and characterized MoS_2 and holey MoS_2 NS. He fabricated the membranes and tested the performance of the membranes. He wrote the first draft of the manuscript. A.C. conducted the Raman spectroscopic measurements and contributed to the production of figures and the manuscript. S.R. and P.C. carried out the computational studies under the supervision of S.K. P.S. measured the contact angles and did the FESEM imaging of the membranes. R.I. and R.K. helped to fabricate and to test the membranes, and J.S.K. carried out antifouling measurements. S.B. helped to prepare holey MoS_2 NS. T.P. suggested the problem, supervised the project, and finalized the manuscript.

Notes

The authors declare no competing financial interest.

■ ACKNOWLEDGMENTS

We thank the Department of Science and Technology, Government of India for constantly supporting our research program on nanomaterials. B.M., P.K., and J.S.K. thank IIT Madras, and A.C. and R.I. thank the CSIR, Govt. of India for their research fellowships. S.K. thanks Anusandhan National Research Foundation (ANRF), India, for the funding through the Core Research Grant (CRG/2022/003771). S.R. thanks the Department of Science and Technology, Government of India, for the INSPIRE fellowship. P.C. thanks the Centre for Atomistic Modelling and Materials Design (CAMMD) Centre of Excellence, IIT Madras, for the postdoctoral fellowship through the IoE scheme. S.K., S.R., and P.C. thank CAMMD and IIT Madras for the HPC facilities. T.P. thanks funding from the Centre of Excellence (CoE) on Molecular Materials and Functions under the Institute of Eminence (IoE) scheme of IIT Madras, Science and Engineering Research Board (SERB), India, for funding through the SPR/2021/000439 research grant and a JC Bose Fellowship.

■ ABBREVIATIONS

NS, nanosheet; FESEM, field emission scanning electron microscopy; TEM, transmission electron microscopy; bM, blank membrane; hMoS_2M, holey MoS_2-based membrane; MoS_2M, MoS_2-based (without holes) membrane; EDS, energy-dispersive spectroscopy; WF, water flux; IR, ion rejection

■ REFERENCES

(1) Shannon, M. A.; Bohn, P. W.; Elimelech, M.; Georgiadis, J. G.; Mariñas, B. J.; Mayes, A. M. Science and Technology for Water Purification in the Coming Decades. *Nature* **2008**, *452* (7185), 301−310.

(2) Elimelech, M.; Phillip, W. A. The Future of Seawater Desalination: Energy, Technology, and the Environment. *Science* **2011**, *333* (6043), 712.

(3) Nagar, A.; Pradeep, T. Clean Water through Nanotechnology: Needs, Gaps, and Fulfillment. *ACS Nano* **2020**, *14* (6), 6420−6435.

(4) Henthorne, L.; Boysen, B. State-of-the-Art of Reverse Osmosis Desalination Pretreatment. *Desalination* **2015**, *356*, 129−139.

(5) UNESCO *Water and Climate Change*; United Nations Educational, Scientific and Cultural Organization: Paris, 2020; S. and C. O., Ed..

(6) Pendergast, M. M.; Hoek, E. M. V. A Review of Water Treatment Membrane Nanotechnologies. *Energy Environ. Sci.* **2011**, *4* (6), 1946−1971.

(7) Werber, J. R.; Osuji, C. O.; Elimelech, M. Materials for Next-Generation Desalination and Water Purification Membranes. *Nat. Rev. Mater.* **2016**, *1* (5), 16018.

(8) Wei, W.; Xiangli, F.; Jin, W.; Xu, N. Solvent Resistant Nanofiltration Membranes. *Prog. Chem.* **2007**, *19*, 1592−1597.

(9) Van der Bruggen, B.; Mänttäri, M.; Nyström, M. Drawbacks of Applying Nanofiltration and How to Avoid Them: A Review. *Sep. Purif. Technol.* **2008**, *63* (2), 251−263.

(10) Condom, S.; Larbot, A.; Alami Younssi, S.; Persin, M. Use of Ultra- and Nanofiltration Ceramic Membranes for Desalination. *Desalination* **2004**, *168*, 207−213.

(11) Zhu, B.; Myat, D. T.; Shin, J.-W.; Na, Y.-H.; Moon, I.-S.; Connor, G.; Maeda, S.; Morris, G.; Gray, S.; Duke, M. Application of Robust MFI-Type Zeolite Membrane for Desalination of Saline Wastewater. *J. Membr. Sci.* **2015**, *475*, 167−174.

(12) Sun, P.; Wang, K.; Zhu, H. Recent Developments in Graphene-Based Membranes: Structure, Mass-Transport Mechanism and Potential Applications. *Adv. Mater.* **2016**, *28* (12), 2287−2310.

(13) Liu, G.; Jin, W.; Xu, N. Two-Dimensional-Material Membranes: A New Family of High-Performance Separation Membranes. *Angew. Chem., Int. Ed.* **2016**, *55* (43), 13384−13397.

(14) Zhao, Y.; Xie, Y.; Liu, Z.; Wang, X.; Chai, Y.; Yan, F. Two-Dimensional Material Membranes: An Emerging Platform for Controllable Mass Transport Applications. *Small* **2014**, *10* (22), 4521−4542.

(15) Deng, M.; Kwac, K.; Li, M.; Jung, Y.; Park, H. G. Stability, Molecular Sieving, and Ion Diffusion Selectivity of a Lamellar Membrane from Two-Dimensional Molybdenum Disulfide. *Nano Lett.* **2017**, *17* (4), 2342−2348.

(16) Sri Abirami Saraswathi, M. S.; Rana, D.; Vijayakumar, P.; Alwarappan, S.; Nagendran, A. Tailored PVDF Nanocomposite Membranes Using Exfoliated MoS2 Nanosheets for Improved Permeation and Antifouling Performance. *New J. Chem.* **2017**, *41* (23), 14315−14324.

(17) Azamat, J.; Khataee, A.; Sadikoglu, F. Computational Study on the Efficiency of MoS2Membrane for Removing Arsenic from Contaminated Water. *J. Mol. Liq.* **2018**, *249*, 110−116.

(18) Zhou, J.; Qin, Z.; Lu, Y.; Li, X.; An, Q.; Ji, S.; Wang, N.; Guo, H. MoS2/Polyelectrolytes Hybrid Nanofiltration (NF) Membranes with Enhanced Permselectivity. *J. Taiwan Inst. Chem. Eng.* **2018**, *84*, 196−202.

(19) Hirunpinyopas, W.; Prestat, E.; Iamprasertkun, P.; Bissett, M. A.; Dryfe, R. A. W. Potential Dependent Ionic Sieving through Functionalized Laminar MoS2Membranes. *2d Mater.* **2020**, *7* (1), 015030.

(20) Sun, L.; Huang, H.; Peng, X. Laminar MoS2Membranes for Molecule Separation. *Chem. Commun.* **2013**, *49* (91), 10718−10720.

(21) Kang, G.; Cao, Y. Development of Antifouling Reverse Osmosis Membranes for Water Treatment: A Review. *Water Res.* **2012**, *46* (3), 584−600.

(22) Wu, B.; Song, Z.; Xiang, Y.; Sun, H.; Yao, H.; Chen, J. Desalination Performance of MoS2Membranes with Different Single-Pore Sizes: A Molecular Dynamics Simulation Study. *ACS Omega* **2024**, *9* (21), 22851−22857.
(23) Dillenburg, R.F.; Abal, J. P. K.; Barbosa, M. C. Computational Investigation on Water and Ion Transport in MoS2 Nanoporous Membranes: Implications for Water Desalination. *ACS Appl. Nano Mater.* **2023**, *6* (6), 4465−4476.
(24) Heiranian, M.; Farimani, A. B.; Aluru, N. R. Water Desalination with a Single-Layer MoS2 Nanopore. *Nat. Commun.* **2015**, *6* (1), 8616.
(25) Opetubo, O.; Kitalu, R.; Oviroh, P.; Oyinbo, S.; Imoisili, P.; Jen, T.-C. A Mini-Review on MoS2Membrane for Water Desalination: Recent Development and Challenges. *Nanotechnol. Rev.* **2023**, *12*, 20220563.
(26) Nawal, N.; Nizam, R.; Das, P.; Morshed, M. M. Desalination Performance of Nano Porous Mos2Membrane on Different Salts of Saline Water: A Molecular Dynamics Study. *arXiv* **2023**, arXiv.2310.05729.
(27) Kleinubing Abal, J. P.; Barbosa, M. C. Molecular Fluid Flow in MoS2 Nanoporous Membranes and Hydrodynamics Interactions. *J. Chem. Phys.* **2021**, *154* (13), 134506.
(28) Barati Farimani, O.; Cao, Z.; Barati Farimani, A. Fast Water Desalination with a Graphene−MoS2 Nanoporous Heterostructure. *ACS Appl. Mater. Interfaces* **2024**, *16* (22), 29355−29363.
(29) Levita, G.; Restuccia, P.; Righi, M. C. Graphene and MoS2 Interacting with Water: A Comparison by Ab Initio Calculations. *Carbon* **2016**, *107*, 878−884.
(30) Song, Z.; Niu, Y.; Yang, J.; Chen, L.; Chen, J. Comparison of Water Desalination Performance of Porous Graphene and MoS2 Nanosheets. *RSC Adv.* **2022**, *12* (42), 27641−27647.
(31) Feng, J.; Liu, K.; Graf, M.; Lihter, M.; Bulushev, R. D.; Dumcenco, D.; Alexander, D. T. L.; Krasnozhon, D.; Vuletic, T.; Kis, A.; Radenovic, A. Electrochemical Reaction in Single Layer MoS2: Nanopores Opened Atom by Atom. *Nano Lett.* **2015**, *15* (5), 3431−3438.
(32) He, Y.; Tsutsui, M.; Zhou, Y.; Miao, X.-S. Solid-State Nanopore Systems: From Materials to Applications. *NPG Asia Mater.* **2021**, *13* (1), 48.
(33) Hoenig, E.; Han, Y.; Xu, K.; Li, J.; Wang, M.; Liu, C. In Situ Generation of (Sub) Nanometer Pores in MoS2Membranes for Ion-Selective Transport. *Nat. Commun.* **2024**, *15* (1), 7911.
(34) Hirunpinyopas, W.; Prestat, E.; Worrall, S. D.; Haigh, S. J.; Dryfe, R. A. W.; Bissett, M. A. Desalination and Nanofiltration through Functionalized Laminar MoS2Membranes. *ACS Nano* **2017**, *11* (11), 11082−11090.
(35) Dines, M. B. Lithium Intercalation via N-Butyllithium of the Layered Transition Metal Dichalcogenides. *Mater. Res. Bull.* **1975**, *10* (4), 287−291.
(36) Zeng, Z.; Yin, Z.; Huang, X.; Li, H.; He, Q.; Lu, G.; Boey, F.; Zhang, H. Single-Layer Semiconducting Nanosheets: High-Yield Preparation and Device Fabrication. *Angew. Chem., Int. Ed.* **2011**, *50* (47), 11093−11097.
(37) Lee, C.; Yan, H.; Brus, L. E.; Heinz, T. F.; Hone, J.; Ryu, S. Anomalous Lattice Vibrations of Single- and Few-Layer MoS2. *ACS Nano* **2010**, *4* (5), 2695−2700.
(38) Mak, K. F.; Lee, C.; Hone, J.; Shan, J.; Heinz, T. F. Atomically Thin ${\mathrm{MoS}}_{2}$: A New Direct-Gap Semiconductor. *Phys. Rev. Lett.* **2010**, *105* (13), 136805.
(39) Sarkar, D.; Mondal, B.; Som, A.; Ravindran, S. J.; Jana, S. K.; Manju, C. K.; Pradeep, T. Holey MoS2 Nanosheets with Photocatalytic Metal Rich Edges by Ambient Electrospray Deposition for Solar Water Disinfection. *Global chall.* **2018**, *2* (12), 1800052.
(40) Mondal, B.; Som, A.; Chakraborty, I.; Baksi, A.; Sarkar, D.; Pradeep, T. Unusual Reactivity of MoS2 Nanosheets. *Nanoscale* **2016**, *8* (19), 10282−10290.
(41) Thompson, A. P.; Aktulga, H. M.; Berger, R.; Bolintineanu, D. S.; Brown, W. M.; Crozier, P. S.; in 't Veld, P. J.; Kohlmeyer, A.; Moore, S. G.; Nguyen, T. D.; Shan, R.; Stevens, M. J.; Tranchida, J.; Trott, C.; Plimpton, S. J. LAMMPS - a Flexible Simulation Tool for Particle-Based Materials Modeling at the Atomic, Meso, and Continuum Scales. *Comput. Phys. Commun.* **2022**, *271*, 108171.
(42) Humphrey, W.; Dalke, A.; Schulten, K. VMD: Visual Molecular Dynamics. *J. Mol. Graphics* **1996**, *14* (1), 33−38.
(43) Levine, B. G.; Stone, J. E.; Kohlmeyer, A. Fast Analysis of Molecular Dynamics Trajectories with Graphics Processing Units—Radial Distribution Function Histogramming. *J. Comput. Phys.* **2011**, *230* (9), 3556−3569.
(44) Giorgino, T. Computing 1-D Atomic Densities in Macromolecular Simulations: The Density Profile Tool for VMD. *Comput. Phys. Commun.* **2014**, *185* (1), 317−322.
(45) Alam, I.; Guiney, L. M.; Hersam, M. C.; Chowdhury, I. Antifouling Properties of Two-Dimensional Molybdenum Disulfide and Graphene Oxide. *Environ. Sci.:Nano* **2018**, *5* (7), 1628−1639.

https://doi.org/10.1021/acsanm.5c05244
ACS Appl. Nano Mater. XXXX, XXX, XXX−XXX